

AZBA: A 3D Adult Zebrafish Brain Atlas for the Digital Age

Justin W. Kenney^{1,2,*§}, Patrick E. Steadman^{2,*}, Olivia Young¹, Meng Ting Shi¹, Maris Polanco¹, Saba Dubaishi¹, Thomas Mueller³, and Paul W. Frankland^{2,4-6,§}

¹Department of Biological Sciences, Wayne State University, Detroit, MI, 48202, USA.

²Program in Neurosciences and Mental Health, The Hospital for Sick Children, Toronto, ON, M5G 1X8, Canada.

³Division of Biology, Kansas State University, Manhattan, KS, 66506, USA.

⁴Department of Physiology, University of Toronto, Toronto, ON, M5S 1A8, Canada

⁵Institute of Medical Sciences, University of Toronto, Toronto, ON, M5S 1A8, Canada

⁶Department of Psychology, University of Toronto, Toronto, ON, M5S 1A8, Canada

*These authors contributed equally to this work

§Corresponding authors

Abstract

Zebrafish have made significant contributions to our understanding of the vertebrate brain and the neural basis of behavior, earning a place as one of the most widely used model organisms in neuroscience. Their appeal arises from the marriage of low cost, early life transparency, and ease of genetic manipulation with a behavioral repertoire that becomes more sophisticated as animals transition from larvae to adults. To further enhance the use of adult zebrafish, we created the first fully segmented three-dimensional digital adult zebrafish brain atlas (AZBA). AZBA was built by combining tissue clearing, light-sheet fluorescence microscopy, and three-dimensional image registration of nuclear and antibody stains. These images were used to guide segmentation of the atlas into over 200 neuroanatomical regions comprising the entirety of the adult zebrafish brain. As an open-source, updatable digital resource, AZBA will significantly enhance the use of adult zebrafish in furthering our understanding of vertebrate brain function in both health and disease.

Introduction

Uncovering general principles of neuroanatomical function and brain-behavior relationships requires the integration of findings across model organisms that range in complexity, organization, and accessibility (Brenowitz and Zakon, 2015; Marder, 2002; Yartsev, 2017). Amongst vertebrate model organisms in neuroscience, zebrafish are relative newcomers that have grown in popularity in recent years (Kenney, 2020; Orger and de Polavieja, 2017). Originally established as a model organism for developmental biology due to ease of domestication, high fecundity, and early life transparency (Parichy, 2015), the increased popularity of zebrafish is driven by recent advancements in brain imaging, molecular genetic manipulation, and behavior. To further enhance the use of zebrafish as an animal model in neuroscience, we created a digital three-dimensional brain atlas (AZBA: adult zebrafish brain atlas). Although several digital atlases exist for larval zebrafish (Kunst et al., 2019; Randlett et al., 2015; Ronneberger et al., 2012; Tabor et al., 2019), no atlas of equivalent detail has been created for adult zebrafish. Adult zebrafish provide several important advantages over larval zebrafish such as a mature and histologically differentiated neuroanatomy and a rich behavioral repertoire that includes long-term associative memory, complex social interactions, and goal-driven behaviors (Gerlai, 2016; Kalueff et al., 2013; Kenney et al., 2017; Nakajo et al., 2020).

Three-dimensional digital brain atlases are essential tools for modern neuroscience because they facilitate lines of inquiry that are not possible with two-dimensional book-based atlases. For example, visualization of the three-dimensional structure of the brain and incorporation of new data or discoveries are difficult, if not impossible, with a print atlas. In contrast, digital atlases enable exploration of brain structures in any arbitrary three-dimensional perspective and can be readily updated to incorporate new information such as patterns of gene expression and anatomical connectivity, as has been done for the mouse (Wang et al., 2020). Such features are important for fields like neurodevelopment and comparative neuroanatomy

that rely on three-dimensional topologies to understand how specific brain regions develop and are conserved across species. A digital atlas would also enhance the use of adult zebrafish in disease modeling by enabling a more comprehensive understanding of how the brain changes in response to insults that occur in neurodevelopmental disorders (Sakai et al., 2018), traumatic brain injury (McCutcheon et al., 2017), neurodegeneration (Xi et al., 2011) and the formation and spreading of gliomas (Idilli et al., 2017). Finally, digital atlases enable automated segmentation of new images, which is essential for whole brain mapping approaches that can lead to unexpected discoveries of regional function (Bahl and Engert, 2020; Kim et al., 2015; Pantoja et al., 2020; Randlett et al., 2019). Whole brain activity mapping also facilitates powerful network approaches to understanding brain (Bassett and Sporns, 2017; Coelho et al., 2018; Vetere et al., 2017; Wheeler et al., 2013), yielding insight into how coordinated brain-wide activity gives rise to behavior.

The generation of an adult zebrafish brain atlas presents several challenges in comparison to the larval brain because the mature brain is opaque and several orders of magnitude larger; this makes traditional whole mount approaches impossible and confocal or wide-field microscopy infeasible. We overcome these roadblocks by exploiting recent developments in histology and microscopy. To enable whole-mount imaging, we rendered adult brains transparent using a tissue clearing approach (iDISCO+) that is compatible with different stains such as small molecules, antibodies, and *in situ* probes (Kramer et al., 2018; Renier et al., 2016). High resolution imaging of samples as large as intact adult brains is not amenable to conventional microscopic techniques, so we turned to light-sheet fluorescence microscopy for rapid large volume imaging with minimal photobleaching (Pitrone et al., 2013; Reynaud et al., 2014). To generate an atlas that minimizes individual variations in neuroanatomy, we registered three-dimensional volumes from multiple animals into the same anatomical space prior to averaging (Lerch et al., 2011). To help guide segmentation and generate insight into the

neurochemical organization of the brain, images from ten different antibody stains were also registered into the same anatomical space. Finally, we performed manual segmentation, delineating the atlas into over 200 neuroanatomical regions, including nuclei and white matter tracts.

Taken together, AZBA is the most comprehensive, detailed, and up to date atlas of the adult zebrafish brain. We have made all averaged images freely available (<https://doi.org/10.5061/dryad.dfn2z351g>) to enable their use in exploring the organization of the zebrafish brain and automated segmentation for activity mapping. By generating this resource using readily available techniques, AZBA can be continuously updated to reflect the latest findings in zebrafish neuroanatomy. We anticipate this becoming an indispensable resource as adult zebrafish continue to gain traction as a model organism in understanding the intricacies of the vertebrate brain.

Results

Overall Strategy

To create an averaged three-dimensional atlas, we developed a sample preparation and analysis pipeline for whole-mount 3D image acquisition and registration (Figure 1). We used a whole-mount preparation to avoid issues with slice-based techniques such as tissue loss, tearing, and distortion. To circumvent the challenge of tissue opacity, we used a rapid organic solvent based tissue clearing technique, iDISCO+ (Renier et al., 2016), that renders brains optically transparent. Because conventional microscopic techniques are not suitable for large volume imaging, we used light-sheet microscopy. Image stacks from individual fish brains were converted to 3D volumes and registered into the same anatomical space prior to averaging. Finally, average 3D images were manually segmented into their constituent brain regions.

Light-sheet Imaging

Tissue clearing using iDISCO+ resulted in transparent brains (Figure 2A). iDISCO+ is compatible with a variety of stains, such as a nuclear stain (TO-PRO), that allowed us to approximate the Nissl stain in the print atlas (Wulliman et al., 1996). Cleared and stained brains were imaged in the horizontal plane with an in-plane resolution of 3.25 μm and an axial step-size of 4 μm (Figure 2B) yielding near-isotropic signals at sufficient resolution to distinguish individual cells. From this collection of images, we generated three-dimensional volumes (Figure 2C) that enabled viewing at any arbitrary angle including the coronal and sagittal planes (Figure 2D). Images were subject to quality-control so that those damaged during dissection were discarded. We retained seventeen sets of nuclear stained and associated autofluorescence images, each of which were transformed into 3D volumes for registration.

3D Image Registration

The atlas was generated by registering images from individual animals into the same space, thereby creating an anatomical average. This approach has been previously used in humans (Klein et al., 2009), mice (Dorr et al., 2008; Steadman et al., 2014), macaques (McLaren et al., 2009) and zebrafish larvae (Kunst et al., 2019; Randlett et al., 2015; Ronneberger et al., 2012; Tabor et al., 2019). We used the contrast from the TO-PRO signal and an image registration pipeline toolkit (Friedel et al., 2014) to perform iterative registration to generate a consensus image (Figure 3). This method begins with a 6-parameter linear registration to rotate and translate the initial image dataset followed by a 12-parameter affine registration to scale, translate, rotate, and shear the dataset with a pair-wise approach to avoid bias by outlier images (Figure 3A). Lastly, an iterative non-linear registration with 6 iterations at subsequently higher resolutions was performed using minctracc (Collins and Evans, 1997). This resulted in a set of linear and non-linear transformations for each TO-PRO image in our dataset from native space to a consensus space and orientation. These transformations were then applied to corresponding autofluorescence images, thereby creating an atlas with averaged images containing TO-PRO and autofluorescence signals (Figure 3B).

Antibody stains

To provide additional guidance for segmentation and generate insight into the neurochemical organization of the adult zebrafish brain, we also acquired images using ten different antibody stains (Figure 4A and Table S1). We sought stains that would identify different cell types in the brain, such as neurons (HuC/D), radial glial cells (glial fibrillary associated protein; GFAP), and proliferating cells (proliferating cell nuclear antigen; PCNA), markers for different neurotransmitters (tyrosine hydroxylase (TH), 5-hydroxytryptamine (5-HT), and choline

acetyltransferase (ChAT)) and calcium binding proteins (parvalbumin (PV), calbindin, and calretinin). Some of these stains, such as TH, 5-HT, ChAT, and calretinin have already been subject to brain-wide analysis, making them useful for guiding segmentation.

Fully realizing the utility of different stains requires images to be brought into the same anatomical space as the previously generated TO-PRO average. To achieve this, during imaging of antibody stains we also acquired autofluorescence images, thereby providing a bridge between the antibody images and the TO-PRO images. Autofluorescence images from antibody stains were registered with the autofluorescence channel of the TO-PRO images, yielding a set of transformations that were used to bring antibody stains into the same anatomical space as the TO-PRO stain (Figure 4B). To generate a representative image for each antibody, we averaged together at least five independent datasets. Our approach resulted in strong correspondence between antibody images and the TO-PRO stain (Figure 4C). The accuracy and utility of this approach is apparent from examining structures known to express high levels of specific enzymes, like TH in the locus coeruleus (Figure 4D; green arrows).

Segmentation

Registered images were used to segment the brain into its constituent parts (Figure 5; see Table S2 for anatomical abbreviations and colors). Segmentation was primarily guided by the seminal atlas of Wullimann and colleagues (1996). Regional boundaries and terminology were updated for parts of the brain that have been subject to more recent analysis such as the telencephalon, hypothalamic regions, and motor nuclei (Mueller et al., 2004; Porter and Mueller, 2020; Rink and Wullimann, 2001). Segmenting large, clearly delineated regions, such as the optic tectum and the cerebellum, was straightforward (Figure 5A). Small nuclei that only appear in one or two slices in the atlas or in images from only one axis proved more challenging. For

such regions, we primarily made use of the coronal axis due to it being the most extensively represented in both the atlas and the literature (Figure 5A, bottom). The horizontal and sagittal planes enabled us to identify the anterior-posterior boundaries (Figure 5A, top and middle). To ensure we captured as many neuronal structures as possible, we made extensive use of a neuronal marker (HuC/D), which allowed us to safely identify many boundaries (Figure S1A). Other challenges included the fact that the original brain atlas contains a significant amount of unsegmented space. We also left this space largely unsegmented, in part because limited current knowledge of the zebrafish brain did not allow us to segment radial domains from their periventricular sites to the pial surface. Identification of tracts was largely based on lack nuclear and neuronal staining since we were unsuccessful in finding a white matter stain compatible with iDISCO+ (e.g. the MLF: Figure 4D, pink arrowheads). We anticipate future work will aid in filling these unsegmented regions with the potential to discover new neuronal circuits and anatomical structures.

Segmentation was also guided by stains with antibodies that have been used in prior studies of the adult zebrafish brain. This includes amines like TH and 5-HT (Kaslin and Panula, 2001; Rink and Wullimann, 2001), ChAT to identify cholinergic neurons and motor nuclei (Mueller et al., 2004), and calcium binding proteins like calretinin (Castro et al., 2006a, 2006b). All of our immunostainings showed high overlap with prior work, establishing the validity of these antibodies (Figures 5B,C, and S1B,C). For example, in the telencephalon we found extensive TH expression in the olfactory bulb (Figure 5B-a), and as a continuous band ventral to the Dc region (Figure 5B-b). As previously reported, TH staining was also elevated in the optic tectum, thalamic, and hypothalamic regions (Figure 5B-c,d), the LC (Figure 5B-e), and in the XLo of the hindbrain (Figure 5B-f). We found 5-HT staining to be more diffuse in regions like the optic tectum and the dorsal part of the telencephalon (Figure 5C-a,b), with pockets of high expression restricted to regions like the PVO (Figure 5C-c), PTN (Figure 5C-d), posterior portion

of the Hc (Figure 5C-e), and the SR (Figure 5C-f). Using ChAT, we could clearly discern staining in places such as the RT (Figure S1B-a), near the TTB (Figure S1B-b), and in the SRN and NLV (Figure S1B-c). ChAT staining was also apparent in several motor nuclei such as the OENr and VIIIm (Figure S1B-d), OENc (Figure S1B-e), and IXm (Figure S1B-e). Finally, examples of high levels of calretinin staining can be seen in the olfactory bulb (Figure S1C-a), the Dm (Figure S1C-b), the PSP and optic tract (Figure S1C-c), optic tectum (Figures S1C-c,d,e), the TLa, SG, TGN, and anterior portion of the DIL (Figure S1C-d) with particularly strong staining in the SGN (Figure S1C-e) and DON (Figure S1C-f).

Our segmentation resulted in a three-dimensional model of the zebrafish brain that can be viewed from any arbitrary angle (Figure 5D). Each nucleus, white matter tract, and ventricle was given a unique abbreviation and color, totaling 217 regions (Table S2). This is more than the 210 regions in the original atlas (Wulliman et al., 1996) due to the inclusion of recently identified regional subdivisions. The full extent of the atlas can be most easily appreciated using ITK-SNAP (Yushkevich et al., 2019), a freely available software package designed for viewing three-dimensional medical images that allows for the simultaneous viewing of the stains and segmentation in the coronal, sagittal, and horizontal planes (Figure 6). All files for exploring AZBA are freely available for use in ITK-SNAP or other programs (<https://doi.org/10.5061/dryad.dfn2z351g>).

Neurochemical organization of the adult zebrafish brain

We used AZBA to generate insight into the neurochemical organization of the adult zebrafish brain using antibody stains that have not previously been subject to brain-wide examination. Parvalbumin (PV) is a calcium binding protein that labels a class of inhibitory interneurons (Celio, 1986). We found several highly concentrated areas of PV staining such as

in the anterior portions of the olfactory bulb (Figure 7A), APN and DAO (Figure 7A-b), the TSc (Figure 7A-c), the DON and VIII of the hindbrain (Figure 6A-f), and very high levels in the ventral portion of the molecular layer of the cerebellum (Figure 7A-d,e) the latter of which likely corresponding with Purkinje and crest cells (Bae et al., 2009).

Prox1 is a homeobox gene critical for regulating neuronal development with widespread expression in larval fish. In juveniles and adult zebrafish, Prox1 expression decreases rapidly and is eventually confined to relatively few regions (Ganz et al., 2012; Pistocchi et al., 2008). In the adult zebrafish pallium Prox1 was reported to be present in the neuronal layer of the DI with more diffuse staining in posterior portion of the Dc, which we also observed (Figure 7B-b). We also observe high levels of Prox1 in the olfactory bulb (Figure 7B-a), the habenula (Figure 7B-b), the Val and hypothalamus (Figure 7B-d), the DIL and the molecular layer of the cerebellum (Figure 7B-e,f).

PCNA is a marker for proliferating cells (Grandel et al., 2006; Wullmann and Puelles, 1999). Consistent with widespread neurogenesis in the adult zebrafish brain, we found PCNA expressed in many neurogenic niches with the highest expression along the midline (Figure 7C). For example, in the telencephalon we noticed a band of high expression along the midline in the ventral telencephalon that begins near the olfactory bulbs (Figure 7C-a) with a second area in the posterior portion corresponding to the PPa (Figure 7C-b). We also saw high levels of expression in parts of the thalamus (VM; Figure 7C-c), the hypothalamus (Hd and posterior portion of Hc) and the valvula, caudal lobe, and molecular layers of the cerebellum (Figure 7C-d,e,f).

Calbindin is a calcium binding protein important for regulating intracellular signaling that is often used in comparative neurological studies (Schmidt, 2012). We found calbindin to be concentrated in the fiber layers of the olfactory bulbs (Figure S1D-a), the Dm in the telencephalon (Figure S1D-b), the VOT (Figure S1D-c), throughout the optic tectum (Figure

S1D-c,d,e), the TLa (Figure S1D-d), SGN (Figure S1D-e), and in the VIII and DON of the hindbrain (Figure S1D-f). Notably, calbindin staining patterns largely overlapped with calretinin (Figure S1C).

GFAP is a marker for non-neuronal cells like astrocytes, radial glial cells, and ependymal cells (Doetsch et al., 1997; Eng et al., 2000). Accordingly, we found GFAP most concentrated near the midline and ventricles (Figure 7D). Pockets of expression were present that were not adjacent to ventricles such as near the entopeduncular nuclei (Figure 7D-a), the habenula and anterior portions of the thalamus (Figure 7D-b) and nuzzled between the NI and TSvl (Figure 7D-d). Throughout the hindbrain, GFAP expression was largely restricted to the edges of the brain with the exception of the IR and dorsolateral edge of the XLo (Figure 7D-e,f).

Discussion

In the present article, we introduce a new resource for the zebrafish community: AZBA, a three-dimensional adult zebrafish brain atlas. This resource will facilitate a wide variety of neurobiological studies using adult zebrafish aimed at dissecting neural circuits of behavior, understanding brain pathology, and discovering novel and conserved neural circuits. We created AZBA by leveraging advances in tissue clearing, light-sheet fluorescent microscopy, and image registration, resulting in the most detailed atlas for adult zebrafish to date. Tissue clearing allowed us to take a whole-mount approach, overcoming the natural opacity of the adult brain and issues associated with slice-based techniques such as tissue loss, tearing, and distortion. Laser fluorescence light-sheet microscopy was used to image the large volume of the zebrafish brain with high resolution and minimal photobleaching. Finally, we used three-dimensional image registration to create images derived from multiple animals and inclusion of ten antibody stains into the same anatomical space. These were then used to guide segmentation of the atlas into 217 different neuroanatomical regions.

AZBA represents a significant departure from two prior adult zebrafish brain atlases. The seminal book atlas from Wullmann and colleagues (1996) is exceptionally detailed and has guided zebrafish neuroscience research for over two decades. However, being in print, it has not been updated with the latest findings and its two-dimensional visual presentation and lack of chemoarchitectural markers makes identifying regional boundaries across anatomical planes problematic. More recently, Ullmann and colleagues used magnetic resonance imaging (MRI) to create a three-dimensional atlas for adult zebrafish (Ullmann et al., 2010). Using a 16.4 Tesla magnet, they imaged a single brain at approximately 10 μm resolution and segmented it into 53 regions. Although an important achievement, MRI is limited in its ability to detect a variety of neurochemical markers and does not integrate easily with genetic labeling techniques. Furthermore, such strong magnets are not readily available to most researchers. In contrast, by

combining recent advances in widely available tissue clearing techniques, light-sheet microscopy, and image registration, AZBA is highly versatile, detailed, and accessible.

Antibody stains were central to developing AZBA because they validated our approach and improved segmentation through comparison to prior work. Indeed, patterns of our neurotransmitter related stains largely agree with previous reports probing TH (Castro et al., 2006b; Kaslin and Panula, 2001; Ma, 2003; Yamamoto et al., 2010), 5-HT (Kaslin and Panula, 2001; Norton et al., 2008), and ChAT (Castro et al., 2006b; Clemente et al., 2004; Mueller et al., 2004). PCNA also overlaps with earlier findings using both PCNA antibodies and bromodeoxyuridine labelling (Ampatzis et al., 2012; Byrd and Brunjes, 2001; Grandel et al., 2006; Ito et al., 2010; Makantasi and Dermon, 2014; von Krogh et al., 2010). Likewise, stains against the calcium binding proteins like calretinin, calbindin, and PV, largely overlap with prior work with only minor exceptions. Consistent with previous studies we find calretinin expressed in the olfactory bulb (Kress et al., 2015), telencephalon (Porter and Mueller, 2020) and posterior parts of the brain, with the only notable exceptions being our lack of staining in the torus semicircularis and perilemniscal nucleus (Castro et al., 2006b, 2006a). For calbindin, despite using the same antibody, we find that our staining in the telencephalon looks different than previous work (von Trotha et al., 2014) where we find little staining in the subpallium, and instead see staining in the medial zone of the dorsal telencephalon limited to its posterior extent. For PV, we also note significant overlap with prior work where we see labelling in cell bodies of the cerebellum and olfactory bulbs, but less consistency in the more diffuse staining in the telencephalon (Ampatzis and Dermon, 2007; Bae et al., 2009; Mueller et al., 2011; Porter and Mueller, 2020). Some of these minor discrepancies may be due to differences in antigenicity arising from the use of different methodologies for fixation, loss of sparse signal due to the averaging of multiple images, tissue distortion (Renier et al., 2016; Richardson and Lichtman, 2015), or because prior work reported images from single animals and may be more susceptible

to individual variation in expression patterns compared to the present work where images are averaged across several animals. Nonetheless, our high correspondence with the previous literature suggests the present work accurately represents the adult zebrafish brain.

Of the antibody stains that had not been subject to extensive prior work, the findings of greatest interest are from Prox1, a homeobox protein critical to the development of an array of organs and cell types including neurons during embryonic and adult stages (Elsir et al., 2012; Kaltezioti et al., 2010; Karalay et al., 2011). We found Prox1 staining in the telencephalon, consistent with prior work (Ganz et al., 2012), as well as the habenula, parts of the hypothalamus, and the cerebellum (Figure 7B). Hypothalamic *Prox1* expression in larval zebrafish has been found to be important for the development of catecholaminergic neurons (Pistocchi et al., 2008). However, we do not see overlap between TH and Prox1 in the hypothalamus, suggesting Prox1 may be important for the development, but not the maintenance, of hypothalamic catecholaminergic neurons. In adult mice, Prox1 is present in the dentate gyrus of the hippocampus and GFAP positive cells localized to white matter tracts in the cerebellum (Karalay et al., 2011; Lavado and Oliver, 2007). Interestingly, we find overlap between Prox1 and GFAP in the olfactory bulb and the edges of the telencephalon, but not the cerebellum, where Prox1 has greater overlap with PCNA, a marker for proliferating cells. The dentate gyrus in mice is notable for being one of the few areas where adult neurogenesis has been demonstrated (Ming and Song, 2011). Thus, the broader expression of Prox1 in our study may reflect the presence of more widespread neurogenesis in adult zebrafish compared to mice (Kizil et al., 2012).

We view the current segmentation and image collection that comprises AZBA as a first version that will be continually updated. We expect future work will incorporate more antibody images and *in situ* hybridization probes for understanding how patterns of protein and gene expression vary across the brain. Through collaboration with the zebrafish community, we plan

to incorporate the wealth of Gal4 and Cre/loxP lines that have been generated to characterize expression patterns in the adult brain. We envision a process where scientists send fixed brain samples to a central lab for tissue clearing, imaging, and registration to the atlas for incorporation into an online resource. A similar approach has been taken with larval fish (Kawakami et al., 2010; Kunst et al., 2019; Randlett et al., 2015; Ronneberger et al., 2012; Tabor et al., 2019). However, inclusion of images from adult animals are important because transgene expression patterns can change as animals mature (Lal et al., 2018).

AZBA also enables new insight into the functional organization of the zebrafish brain by facilitating whole-brain activity mapping as has been achieved with larval zebrafish (Ahrens et al., 2012; Randlett et al., 2015). New images can be automatically segmented into individual brain regions by registration to our averaged autofluorescence or nuclear stained images (Figure 4). Because adult zebrafish have a mature neuroanatomy and a larger behavioral repertoire than larval fish, this will provide an important new avenue for exploiting the power of the zebrafish model system to yield insight into the functional organization of the vertebrate brain and how it relates to behavior.

AZBA provides an unprecedented view of the adult zebrafish brain, consisting of averaged three-dimensional nuclear stained and antibody images registered into the same space. All files associated with the atlas are available to the community (<https://doi.org/10.5061/dryad.dfn2z351g>) and can be viewed with ITK-SNAP, a freely available software package (Yushkevich et al., 2019). With AZBA, adult zebrafish join the ranks of other vertebrate model organisms in neuroscience that have highly detailed digital atlases such as larval zebrafish (Kunst et al., 2019; Randlett et al., 2015; Ronneberger et al., 2012; Tabor et al., 2019), mice (Lein et al., 2007), and rhesus macaques (Reveley et al., 2016). We anticipate AZBA will contribute to the ascent of adult zebrafish into the upper echelons of model organisms

in neuroscience and contribute to our understanding of the evolution, development, and functioning of the vertebrate central nervous system.

Acknowledgments

We thank Maria Palazzolo for help with preparing the atlas. We thank Angela Morley, Alan Ng, Monica Yu, and Hillary Winstanley for excellent care of the zebrafish, and we thank Tod Thiele for helpful comments on the manuscript. This work was supported by the Human Frontiers Science Program (HFSP; LT000759/2014) and Wayne State University Start-up funds to J.W.K, the Canadian Institute for Health Research to P.W.F. (FDN143227). P.W.F is a senior fellow in the Canadian Institute for Advanced Research program in Child and Brain Development. T.M. was supported by the Cognitive and Neurobiological Approaches to Plasticity Center, a Center of Biomedical Research Excellence of the National Institutes of Health (P20GM113109) and by the HFSP (RGP0016/2019).

Methods

Subjects

Subjects were AB fish (15-16 weeks of age) of both sexes. Fish were housed in 2 L tanks with 8-12 fish per tank. All fish were bred and raised at the Hospital for Sick Children in high density racks with a 14:10 light/dark cycle (lights on at 8:30) and fed twice daily with *Artemia salina*. All procedures were approved by the Hospital for Sick Children Animal Care and Use Committee.

Sample preparation

Zebrafish were euthanized by anesthetizing in 4% tricaine followed by immersion in ice cold water for five minutes. Animals were then decapitated using a razor blade and heads were placed in ice cold PBS for five minutes to let blood drain. Heads were then fixed in 4% PFA overnight after which brains were then carefully dissected into cold PBS and stored at 4 C until processing for iDISCO+. Brains that were damaged during the dissection process were not used for generating the atlas.

Tissue staining

Tissue staining and clearing was performed using iDISCO+ (Renier et al., 2016). Samples were first washed three times in PBS at room temperature, followed by dehydration in a series of methanol/water mixtures (an hour each in 20%, 40%, 60%, 80%, 100% methanol). Samples were further washed in 100% methanol, chilled on ice, and then incubated in 5% hydrogen peroxide in methanol overnight at 4 C. The next day, samples were rehydrated in a methanol/water series at room temperature (80%, 60%, 40%, 20% methanol) followed by a PBS wash and two one-hour washes in PTx.2 (PBS with 0.2% TritonX-100). Samples were then

washed overnight at 37 C in permeabilization solution (PBS with 0.2% TritonX-100, 0.3 M glycine, 20% DMSO) followed by an overnight incubation at 37 C in blocking solution (PBS with 0.2% TritonX-100, 6% normal donkey serum, and 10% DMSO). Samples were then labelled with TO-PRO3 iodide (TO-PRO) (1 night) or primary antibodies (2-3 nights) via incubation at 37 C in PTwH (PTx.2 with 10 µg/mL heparin) with 3% donkey serum and 5% DMSO. Samples were then washed at 37 C for one day with five changes of PTwH. Antibody stained samples were followed by incubation with secondary antibodies at 37 C for 2-3 days in PTwH with 3% donkey serum. For samples labelled with TO-PRO, the secondary antibody labelling step was omitted. Following secondary antibody labelling, samples were again washed at 37 C in PTwH for one day with five solution changes.

Tissue clearing

Labelled brains were first dehydrated in a series of methanol water mixtures at room temperature (an hour each in 20%, 40%, 60%, 80%, 100% (x2) methanol) and then left overnight in 100% methanol. Samples were then incubated at room temperature in 66% dichloromethane in methanol for three hours followed by two 15-minute washes in dichloromethane. After removal of dichloromethane, samples were incubated and stored in dibenzyl ether until imaging.

Imaging

All imaging was done on a LaVision ultramicroscope I. Samples were mounted using an ultraviolet curing resin (adhesive 61 from Norland Optical, Cranbury, NJ) that had a refractive index (1.56) that matched the imaging solution, dibenzyl ether. Images were acquired in the horizontal plane at 4X magnification.

Image processing

Data sets from light sheet imaging were stitched using Fiji's (NIH) extension for Grid Stitching (Preibisch et al., 2009) and converted to a single stack, corresponding to the z-axis. All image processing steps were run on a Linux-workstation with 64 GB of RAM and 12-core Intel processor.

Each stack was converted to a 4 μm isotropic image using custom python code with separate files for the autofluorescence channel and a second for the antibody or TO-PRO channels. These images were resampled to 8 μm isotropic due to system constraints during the image registration stages.

Registration

The autofluorescence signal was acquired on an initial dataset of 17 brains along with the nuclear marker, TO-PRO. To create the initial average, we used image registration to align in a parallel group-wise fashion the TO-PRO images. The variability was expected to be less in the TO-PRO because these images contained more contrast than the autofluorescence images.

The creation of an initial average of the adult zebrafish brain was accomplished using 17 samples with the TO-PRO channel. The process was completed using a 3-step registration process, similar to prior work (Lerch et al., 2011) using the pydpiper pipeline framework (Friedel et al., 2014) and the minctracc registration tool (Collins and Evans, 1997). This involved taking a single sample at random and registering the 17 samples to it using a 6-parameter linear alignment process (LSQ6). This yielded 17 samples in similar orientation to allow a 12-parameter linear registration (LSQ12) to be performed in a pair-wise fashion (each sample is paired with all the other samples, to avoid sample bias) and the final output of these 12-

parameter registration was a group average. This represents a linearly registered average adult zebrafish brain. This was then used as the target for non-linear registration with each of the linearly registered 17 TO-PRO samples. This non-linear alignment was repeated successively with smaller step sizes and blurring kernels to allow for an average with minimal bias from any one sample brain. We then took this average and mirrored itself along the long axis of the brain and repeated the registration process described above but instead of using a random brain as the 6-parameter target, we used this mirrored brain. The result of this second pipeline was an average brain where each plane of the brain (coronal, sagittal, horizontal) are parallel with the same planes of the image (i.e. it created a symmetric, centered brain). This final average brain represented the starting point of the atlas. The linear and non-linear transformations created in the registration pipeline were used to resample the 4 μm isotropic TO-PRO and autofluorescence images to the atlas space, yielding an average signal for each channel. The autofluorescence signal was used to register other sample datasets with the atlas because it is common across all datasets.

To combine the additional cellular markers to better delineate structures and examine their distribution across the brain, we converted all images and their channels to 4 μm isotropic images as described above. We then converted them to 8 μm isotropic and used the autofluorescence channel for each set to run the above registration pipeline (LSQ6, LSQ12 and non-linear). The initial target was the autofluorescence average created with the TO-PRO dataset described above. Following each registration pipeline, the transformations were used to resample each autofluorescence and cellular marker channel to the atlas with a resolution of 4 μm isotropic.

Segmentation

Segmentation was performed using ITK-SNAP, a freely available software package for working with multimodal medical images that enables side-by-side viewing of 3D images registered into the same anatomical space (Yushkevich et al., 2019). Segmentation was primarily guided by comparing TO-PRO nuclear stained images to the cresyl violet stain of the original atlas (Wullimann et al., 1996). Boundaries of nuclei were often determined using the TO-PRO stain in conjunction with a neuronal marker (HuC/D) and other antibody stains as needed. Terminology largely follows that of the original atlas with the exception of motor nuclei (Mueller et al., 2004) and the telencephalon (Porter and Mueller, 2020).

Figures

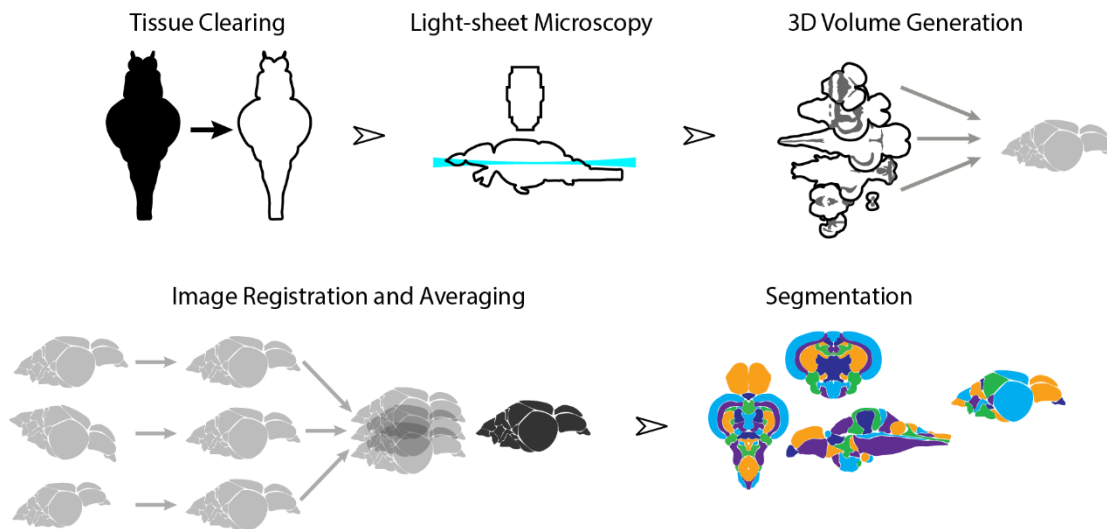


Figure 1. Overview of the strategy for generating AZBA. Dissected brain samples were first subject to staining and tissue clearing. This was followed by whole-mount imaging using light-sheet fluorescence microscopy. Three-dimensional volumes were created from individual image sets, and then registered into the same anatomical space prior to averaging to generate a representative image. Finally, volumes were segmented into over 200 neuronal nuclei and white matter tracts.

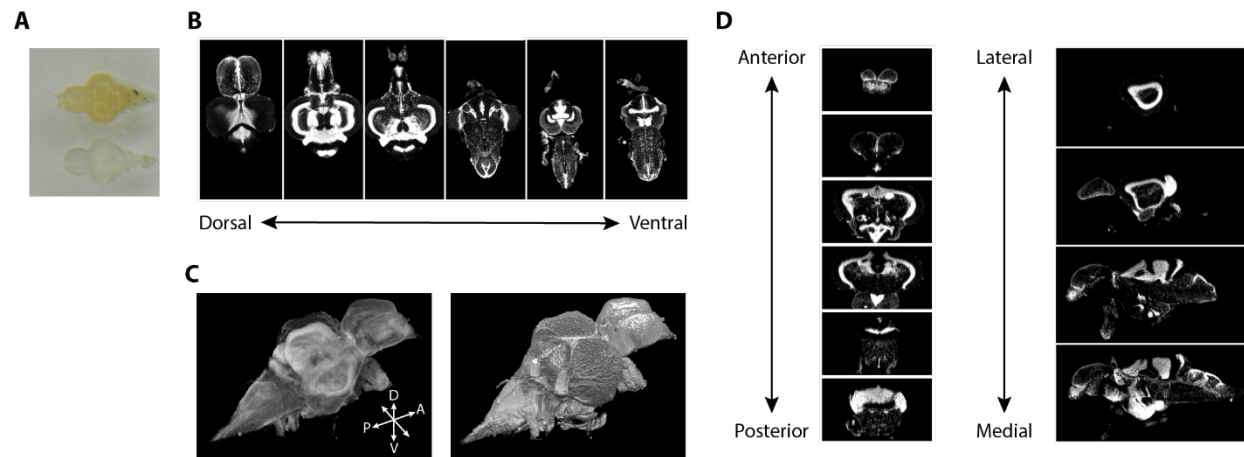


Figure 2. Imaging of nuclear stained tissue-cleared samples. **A)** Image of adult zebrafish brain samples before (top) and after (bottom) clearing using iDISCO+. **B)** Example TO-PRO stained images from a single sample acquired in the horizontal plane during light-sheet imaging. **C)** Three-dimensional volumes generated from a set of light-sheet images from an individual brain visualized using a maximum intensity projection (left), and exterior volume (right). **D)** Coronal (left) and sagittal (right) views of an individual brain generated from a single three-dimensional volume.

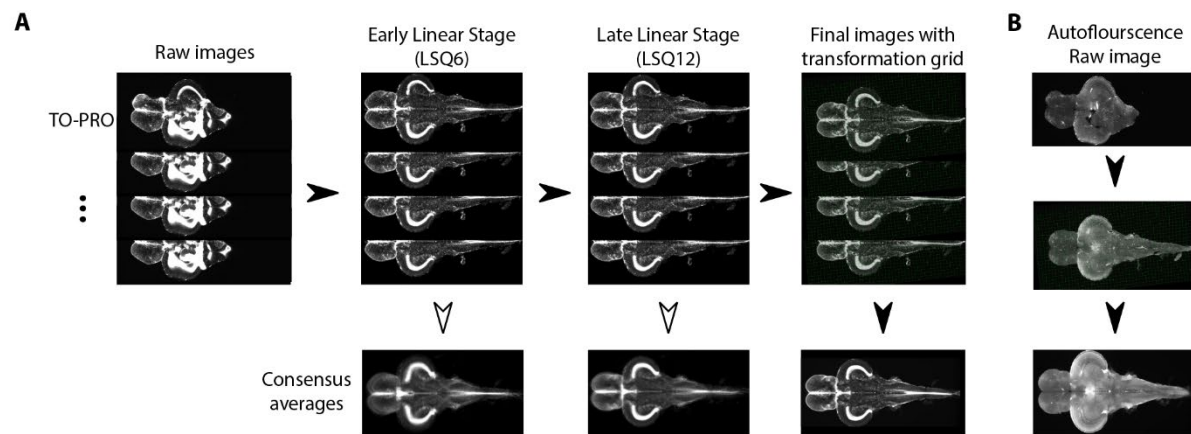


Figure 3. Image registration pipeline. **A)** Raw TO-PRO images from 17 fish were first aligned using linear transformations (LSQ6 and LSQ12) followed by a final non-linear transformation (right). Deformation grids at each stage are overlaid. Consensus average images at each stage of the pipeline are below. **B)** Raw autofluorescence images (top) acquired at the same time as the TO-PRO images were registered into the same space using the transformations derived from TO-PRO registration (middle). Images were then averaged together to generate a corresponding autofluorescence average in the same anatomical space as the TO-PRO images (bottom).

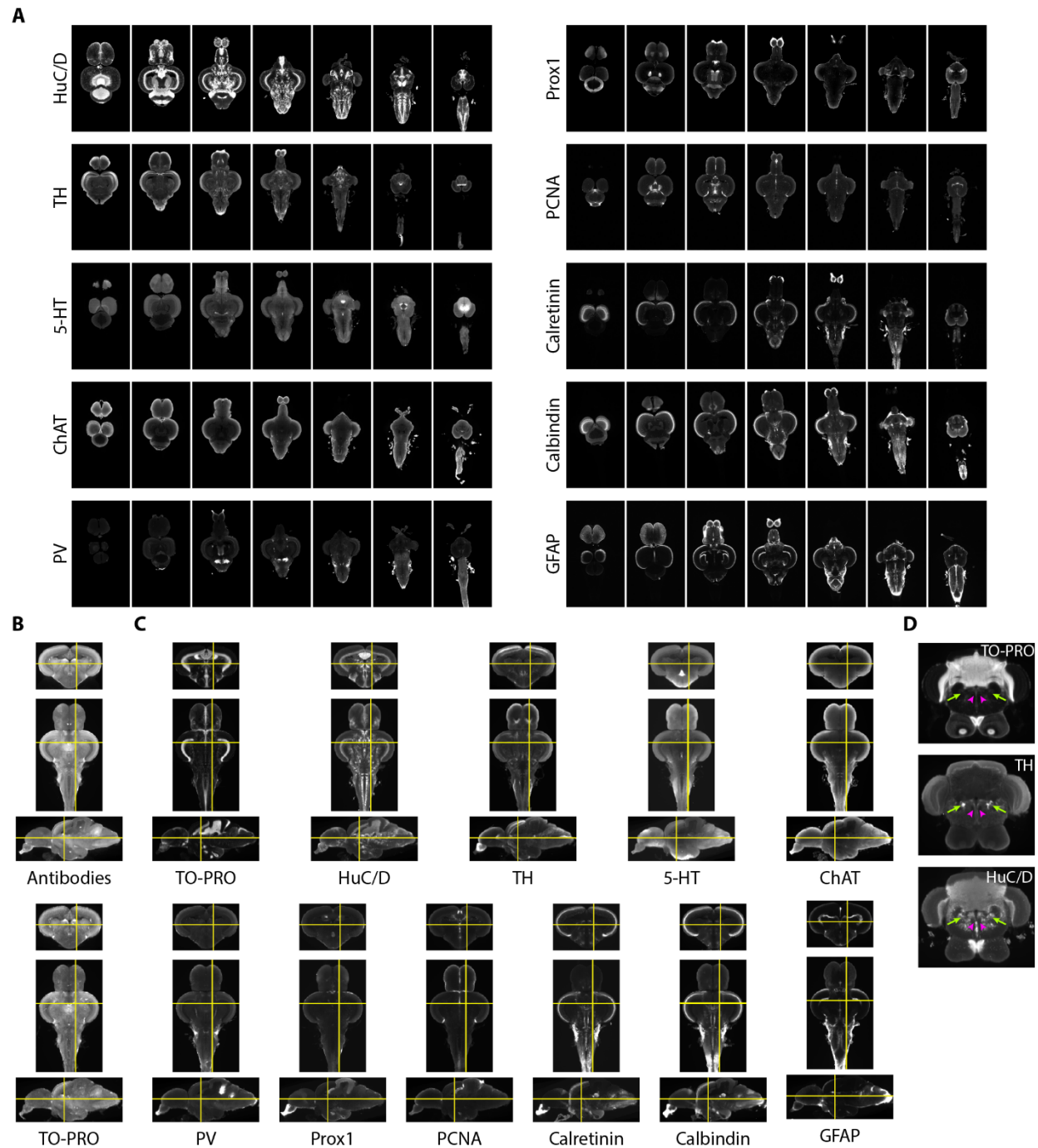


Figure 4. Imaging and registration of antibody stains. **A)** Representative light-sheet images taken in the horizontal plane from individual brains stained with indicated antibodies. **B)** Autofluorescence images acquired during antibody staining (top) were registered into the same space as autofluorescence images acquired during TO-PRO staining (bottom). **C)** Transformations from autofluorescence registration were applied to antibody images to bring antibody stains into the same anatomical space as the TO-PRO stain. Yellow crosshairs are in the same place on each image. **D)** Example of correspondence between TO-PRO and antibody images and how stains can be used to identify the boundaries of specific nuclei (green arrow:

locus coeruleus) and white matter tracts by a lack of staining (pink arrowhead: medial longitudinal fascicle).

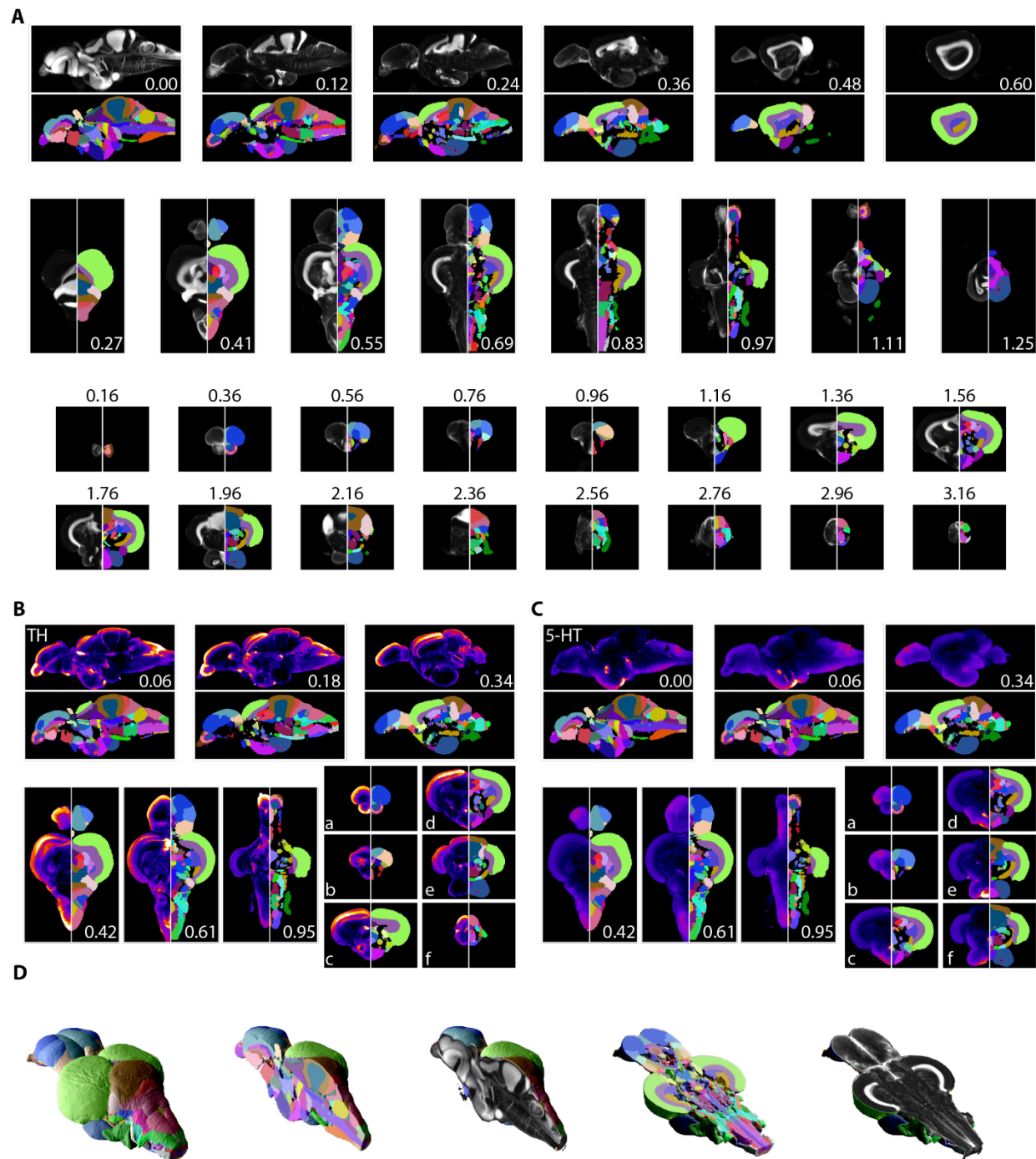


Figure 5. Segmentation of AZBA. **A)** Averaged and registered TO-PRO images alongside the atlas segmentation. For sagittal (top), horizontal (middle), and coronal (bottom) planes numbers are distance (in mm) from the midline, top, and anterior most portion of the brain, respectively. **B and C)** Averaged and registered TH and 5-HT stained images where hotter colors indicate a stronger signal. Numbers same as in (A). Slices in each plane were chosen to show regions

containing high levels of staining (see results for description). **D)** Three-dimensional representation of the segmentation with a sagittal and horizontal cutaway overlaid with TO-PRO the TO-PRO stain of the atlas.

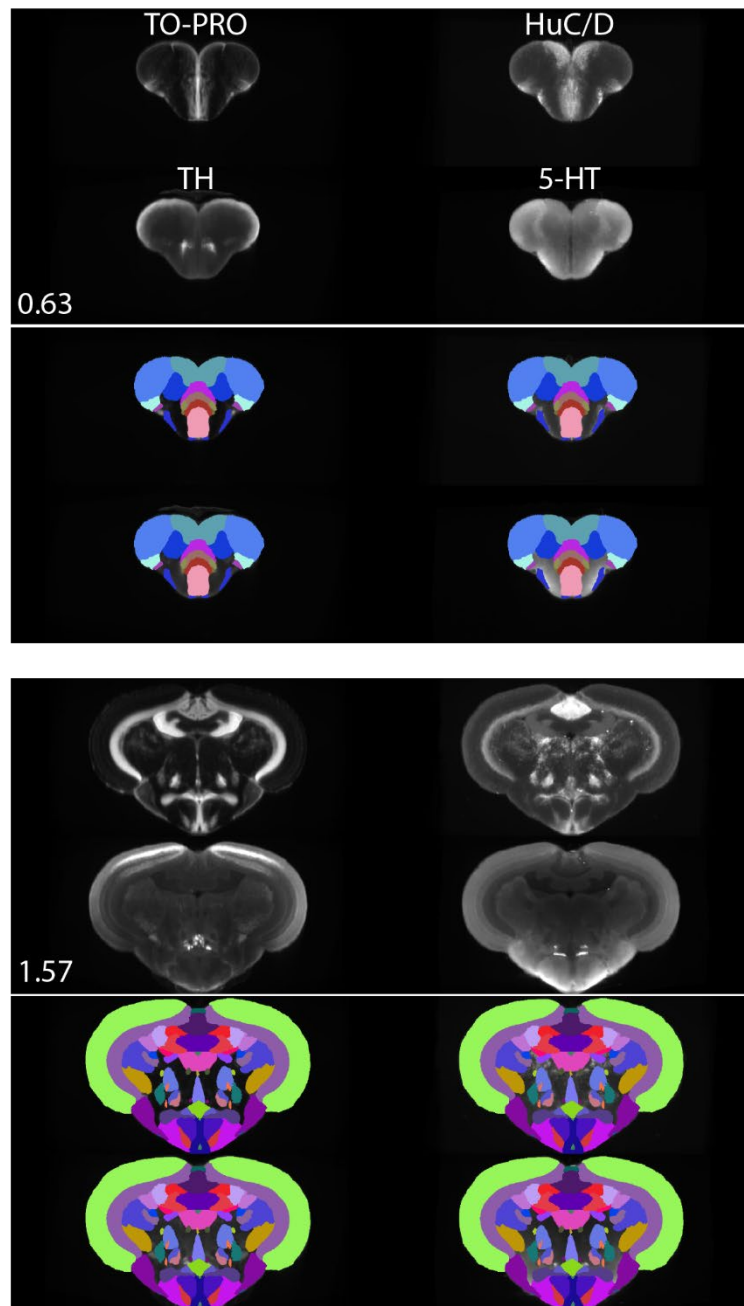


Figure 6. Registered and averaged TO-PRO, HuC/D, TH, and 5-HT images in the coronal plane alongside atlas segmentation. Numbers are distance (in mm) from the anterior most portion of the brain.

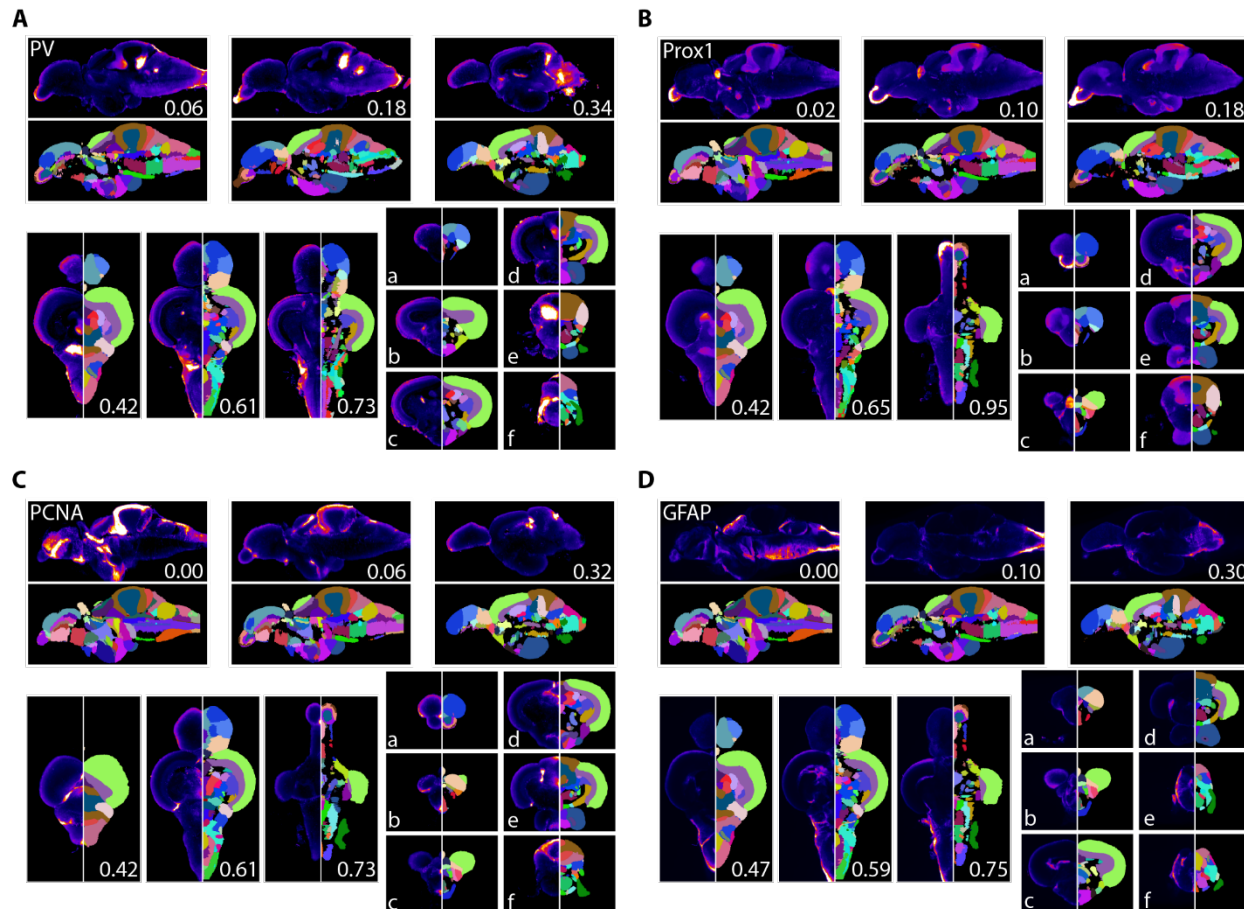


Figure 7. Averaged and registered antibody stains with corresponding segmentation for **A) PV**, **B) Prox1**, **C) PCNA**, and **D) GFAP** where hotter colors indicate greater staining. For sagittal (top) and horizontal (left, bottom) numbers represent distance (in mm) from midline or top of the brain, respectively. Slices for each plane were chosen based on the presence of staining (see results for description).

References

- Ahrens MB, Li JM, Orger MB, Robson DN, Schier AF, Engert F, Portugues R. 2012. Brain-wide neuronal dynamics during motor adaptation in zebrafish. *Nature* **485**:471–477. doi:10.1038/nature11057
- Ampatzis K, Dermon CR. 2007. Sex differences in adult cell proliferation within the zebrafish (*Danio rerio*) cerebellum. *Eur J Neurosci* **25**:1030–1040. doi:10.1111/j.1460-9568.2007.05366.x
- Ampatzis K, Makantasi P, Dermon CR. 2012. Cell proliferation pattern in adult zebrafish forebrain is sexually dimorphic. *Neuroscience* **226**:367–381. doi:10.1016/j.neuroscience.2012.09.022
- Bae YK, Kani S, Shimizu T, Tanabe K, Nojima H, Kimura Y, Higashijima S ichi, Hibi M. 2009. Anatomy of zebrafish cerebellum and screen for mutations affecting its development. *Dev Biol* **330**:406–426. doi:10.1016/j.ydbio.2009.04.013
- Bahl A, Engert F. 2020. Neural circuits for evidence accumulation and decision making in larval zebrafish. *Nat Neurosci* **23**:94–102. doi:10.1038/s41593-019-0534-9
- Bassett DS, Sporns O. 2017. Network neuroscience. *Nat Neurosci* **20**:353–364. doi:10.1038/nn.4502
- Brenowitz EA, Zakon HH. 2015. Emerging from the bottleneck: Benefits of the comparative approach to modern neuroscience. *Trends Neurosci* **38**:273–278. doi:10.1016/j.tins.2015.02.008
- Byrd CA, Brunjes PC. 2001. Neurogenesis in the olfactory bulb of adult zebrafish. *Neuroscience* **105**:793–801. doi:10.1016/S0306-4522(01)00215-9
- Castro A, Becerra M, Manso MJ, Anadón R. 2006a. Calretinin immunoreactivity in the brain of the zebrafish, *Danio rerio*: Distribution and comparison with some neuropeptides and neurotransmitter- synthesizing enzymes. II. Midbrain, hindbrain, and rostral spinal cord. *J Comp Neurol* **494**:792–814. doi:10.1002/cne.20843
- Castro A, Becerra M, Manso MJ, Anadón R. 2006b. Calretinin immunoreactivity in the brain of the zebrafish, *Danio rerio*: Distribution and comparison with some neuropeptides and neurotransmitter- synthesizing enzymes. I. Olfactory organ and forebrain. *J Comp Neurol* **494**:435–459. doi:10.1002/cne.20782
- Celio MR. 1986. Parvalbumin in most γ -aminobutyric acid-containing neurons of the rat cerebral cortex. *Science (80-)* **231**:995–997. doi:10.1126/science.3945815
- Clemente D, Porteros Á, Weruaga E, Alonso JR, Arenzana FJ, Aijón J, Arévalo R. 2004. Cholinergic elements in the zebrafish central nervous system: Histochemical and immunohistochemical analysis. *J Comp Neurol* **474**:75–107. doi:10.1002/cne.20111
- Coelho CAO, Ferreira TL, Kramer-Soares JC, Sato JR, Oliveira MGM. 2018. Network supporting contextual fear learning after dorsal hippocampal damage has increased dependence on retrosplenial cortex. *PLOS Comput Biol* **14**:e1006207. doi:10.1371/journal.pcbi.1006207
- Collins DL, Evans AC. 1997. Animal: Validation and application of nonlinear registration-based segmentation. *Int J Pattern Recognit Artif Intell* **11**:1271–1294. doi:10.1142/s0218001497000597

- Doetsch F, García-Verdugo JM, Alvarez-Buylla A. 1997. Cellular composition and three-dimensional organization of the subventricular germinal zone in the adult mammalian brain. *J Neurosci* **17**:5046–5061. doi:10.1523/jneurosci.17-13-05046.1997
- Dorr AE, Lerch JP, Spring S, Kabani N, Henkelman RM. 2008. High resolution three-dimensional brain atlas using an average magnetic resonance image of 40 adult C57Bl/6J mice. *Neuroimage* **42**:60–69. doi:10.1016/j.neuroimage.2008.03.037
- Elsir T, Smits A, Lindström MS, Nistér M. 2012. Transcription factor PROX1: Its role in development and cancer. *Cancer Metastasis Rev.* doi:10.1007/s10555-012-9390-8
- Eng LF, Ghirnikar RS, Lee YL. 2000. Glial Fibrillary Acidic Protein : GFAP-Thirty-One Years (1969 – 2000) * **25**:1439–1451.
- Friedel M, van Eede MC, Pipitone J, Chakravarty MM, Lerch JP. 2014. Pydpipe: a flexible toolkit for constructing novel registration pipelines. *Front Neuroinform* **8**:67. doi:10.3389/fninf.2014.00067
- Ganz J, Kaslin J, Freudenreich D, Machate A, Geffarth M, Brand M. 2012. Subdivisions of the adult zebrafish subpallium by molecular marker analysis. *J Comp Neurol* **520**:633–655. doi:10.1002/cne.22757
- Gerlai R. 2016. Learning and memory in zebrafish (*Danio rerio*). *Methods Cell Biol* **134**:551–586. doi:10.1016/bs.mcb.2016.02.005
- Grandel H, Kaslin J, Ganz J, Wenzel I, Brand M. 2006. Neural stem cells and neurogenesis in the adult zebrafish brain: Origin, proliferation dynamics, migration and cell fate. *Dev Biol* **295**:263–277. doi:10.1016/j.ydbio.2006.03.040
- Idilli AI, Precazzini F, Mione MC, Anelli V. 2017. Zebrafish in Translational Cancer Research: Insight into Leukemia, Melanoma, Glioma and Endocrine Tumor Biology. *Genes (Basel)* **8**:236. doi:10.3390/genes8090236
- Ito Y, Tanaka H, Okamoto H, Ohshima T. 2010. Characterization of neural stem cells and their progeny in the adult zebrafish optic tectum. *Dev Biol* **342**:26–38. doi:10.1016/j.ydbio.2010.03.008
- Kaltezioti V, Kouroupi G, Oikonomaki M, Mantouvalou E, Stergiopoulos A, Charonis A, Rohrer H, Matsas R, Politis PK. 2010. Prox1 Regulates the Notch1-Mediated Inhibition of Neurogenesis. *PLoS Biol* **8**:e1000565. doi:10.1371/journal.pbio.1000565
- Kalueff A V., Gebhardt M, Stewart AM, Cachat JM, Brimmer M, Chawla JS, Craddock C, Kyzar EJ, Roth A, Landsman S, Gaikwad S, Robinson K, Baatrup E, Tierney K, Shamchuk A, Norton W, Miller N, Nicolson T, Braubach O, Gilman CP, Pittman J, Rosenberg DB, Gerlai R, Echevarria D, Lamb E, Neuhauss SCFF, Weng W, Bally-Cuif L, Schneider H, Schneider, and the Zebrafish Neuros H. 2013. Towards a comprehensive catalog of zebrafish behavior 1.0 and beyond. *Zebrafish* **10**:70–86. doi:10.1089/zeb.2012.0861
- Karalay Ö, Doberauer K, Vadodaria KC, Knobloch M, Berti L, Miquelajauregui A, Schwark M, Jagasia R, Taketo MM, Tarabykin V, Lie DC, Jessberger S. 2011. Prospero-related homeobox 1 gene (Prox1) is regulated by canonical Wnt signaling and has a stage-specific role in adult hippocampal neurogenesis. *Proc Natl Acad Sci U S A* **108**:5807–5812. doi:10.1073/pnas.1013456108
- Kaslin J, Panula P. 2001. Comparative anatomy of the histaminergic and other aminergic systems in zebrafish (*Danio rerio*). *J Comp Neurol* **440**:342–377. doi:10.1002/cne.1390

- Kawakami K, Abe G, Asada T, Asakawa K, Fukuda R, Ito A, Lal P, Mouri N, Muto A, Suster ML, Takakubo H, Urasaki A, Wada H, Yoshida M. 2010. zTrap: zebrafish gene trap and enhancer trap database. *BMC Dev Biol* **10**:105. doi:10.1186/1471-213X-10-105
- Kenney JW. 2020. Associative and nonassociative learning in adult zebrafish Behavioral and Neural Genetics of Zebrafish. Elsevier. pp. 187–204. doi:10.1016/b978-0-12-817528-6.00012-7
- Kenney JW, Scott IC, Josselyn SA, Frankland PW. 2017. Contextual fear conditioning in zebrafish. *Learn Mem* **24**:516–523. doi:10.1101/lm.045690.117
- Kim Y, Venkataraju KU, Pradhan K, Mende C, Taranda J, Turaga SC, Arganda-Carreras I, Ng L, Hawrylycz MJ, Rockland KS, Seung HS, Osten P. 2015. Mapping social behavior-induced brain activation at cellular resolution in the mouse. *Cell Rep* **10**:292–305. doi:10.1016/j.celrep.2014.12.014
- Kim Y, Yang GR, Pradhan K, Venkataraju KU, Bota M, García del Molino LC, Fitzgerald G, Ram K, He M, Levine JM, Mitra P, Huang ZJ, Wang XJ, Osten P. 2017. Brain-wide Maps Reveal Stereotyped Cell-Type-Based Cortical Architecture and Subcortical Sexual Dimorphism. *Cell* **171**:456-469.e22. doi:10.1016/j.cell.2017.09.020
- Kizil C, Kaslin J, Kroehne V, Brand M. 2012. Adult neurogenesis and brain regeneration in zebrafish. *Dev Neurobiol* **72**:429–461. doi:10.1002/dneu.20918
- Klein A, Andersson J, Ardekani BA, Ashburner J, Avants B, Chiang MC, Christensen GE, Collins DL, Gee J, Hellier P, Song JH, Jenkinson M, Lepage C, Rueckert D, Thompson P, Vercauteren T, Woods RP, Mann JJ, Parsey R V. 2009. Evaluation of 14 nonlinear deformation algorithms applied to human brain MRI registration. *Neuroimage* **46**:786–802. doi:10.1016/j.neuroimage.2008.12.037
- Kramer EE, Steadman PE, Epp JR, Frankland PW, Josselyn SA. 2018. Assessing Individual Neuronal Activity Across the Intact Brain: Using Hybridization Chain Reaction (HCR) to Detect *Arc* mRNA Localized to the Nucleus in Volumes of Cleared Brain Tissue. *Curr Protoc Neurosci* **84**:e49. doi:10.1002/cpns.49
- Kress S, Biechl D, Wullimann MF. 2015. Combinatorial analysis of calcium-binding proteins in larval and adult zebrafish primary olfactory system identifies differential olfactory bulb glomerular projection fields. *Brain Struct Funct* **220**:1951–1970. doi:10.1007/s00429-014-0765-1
- Kunst M, Laurell E, Mokayes N, Kramer A, Kubo F, Fernandes AM, Förster D, Dal Maschio M, Baier H. 2019. A Cellular-Resolution Atlas of the Larval Zebrafish Brain. *Neuron* **103**:21-38.e5. doi:10.1016/j.neuron.2019.04.034
- Lal P, Tanabe H, Suster ML, Ailani D, Kotani Y, Muto A, Itoh M, Iwasaki M, Wada H, Yaksi E, Kawakami K. 2018. Identification of a neuronal population in the telencephalon essential for fear conditioning in zebrafish. *BMC Biol* **16**. doi:10.1186/s12915-018-0502-y
- Lavado A, Oliver G. 2007. Prox1 expression patterns in the developing and adult murine brain. *Dev Dyn* **236**:518–524. doi:10.1002/dvdy.21024
- Lein ES, Hawrylycz MJ, Ao N, Ayres M, Bensinger A, Bernard A, Boe AF, Boguski MS, Brockway KS, Byrnes EJ, Chen L, Chen TM, Chin MC, Chong J, Crook BE, Czaplinska A, Dang CN, Datta S, Dee NR, Desaki AL, Desta T, Diep E, Dolbeare TA, Donelan MJ, Dong HW, Dougherty JG, Duncan BJ, Ebbert AJ, Eichele G, Estin LK, Faber C, Facer BA, Fields

- R, Fischer SR, Fliss TP, Frensley C, Gates SN, Glattfelder KJ, Halverson KR, Hart MR, Hohmann JG, Howell MP, Jeung DP, Johnson RA, Karr PT, Kawal R, Kidney JM, Knapik RH, Kuan CL, Lake JH, Laramie AR, Larsen KD, Lau C, Lemon TA, Liang AJ, Liu Y, Luong LT, Michaels J, Morgan JJ, Morgan RJ, Mortrud MT, Mosqueda NF, Ng LL, Ng R, Orta GJ, Overly CC, Pak TH, Parry SE, Pathak SD, Pearson OC, Puchalski RB, Riley ZL, Rockett HR, Rowland SA, Royall JJ, Ruiz MJ, Sarno NR, Schaffnit K, Shapovalova N V, Sivasay T, Slaughterbeck CR, Smith SC, Smith KA, Smith BI, Sodt AJ, Stewart NN, Stumpf KR, Sunkin SM, Sutram M, Tam A, Teemer CD, Thaller C, Thompson CL, Varnam LR, Visel A, Whitlock RM, Wohnoutka PE, Wolkey CK, Wong VY, Wood M, Yaylaoglu MB, Young RC, Youngstrom BL, Yuan XF, Zhang B, Zwingman TA, Jones AR. 2007. Genome-wide atlas of gene expression in the adult mouse brain. *Nature* **445**:168–176.
- Lerch JP, Sled JG, Henkelman RM. 2011. MRI phenotyping of genetically altered mice. *Methods Mol Biol* **711**:349–361. doi:10.1007/978-1-61737-992-5_17
- Ma PM. 2003. Catecholaminergic systems in the zebrafish. IV. Organization and projection pattern of dopaminergic neurons in the diencephalon. *J Comp Neurol* **460**:13–37. doi:10.1002/cne.10544
- Makantasi P, Dermon CR. 2014. Estradiol treatment decreases cell proliferation in the neurogenic zones of adult female zebrafish (Danio Rerio) brain. *Neuroscience* **277**:306–320. doi:10.1016/j.neuroscience.2014.06.071
- Marder E. 2002. Non-mammalian models for studying neural development and function. *Nature* **417**:318–321. doi:10.1038/417318a
- McCutcheon V, Park E, Liu E, Sobhebidari P, Tavakkoli J, Wen X-Y, Baker AJ. 2017. A Novel Model of Traumatic Brain Injury in Adult Zebrafish Demonstrates Response to Injury and Treatment Comparable with Mammalian Models. *J Neurotrauma* **34**:1382–1393. doi:10.1089/neu.2016.4497
- McLaren DG, Kosmatka KJ, Oakes TR, Kroenke CD, Kohama SG, Matochik JA, Ingram DK, Johnson SC. 2009. A population-average MRI-based atlas collection of the rhesus macaque. *Neuroimage* **45**:52–59. doi:10.1016/j.neuroimage.2008.10.058
- Ming G li, Song H. 2011. Adult Neurogenesis in the Mammalian Brain: Significant Answers and Significant Questions. *Neuron*. doi:10.1016/j.neuron.2011.05.001
- Mueller T, Dong Z, Berberoglu MA, Guo S. 2011. The dorsal pallium in zebrafish, Danio rerio (Cyprinidae, Teleostei). *Brain Res* **1381**:95–105. doi:10.1016/j.brainres.2010.12.089
- Mueller T, Vernier P, Wullmann MF. 2004. The adult central nervous cholinergic system of a neurogenetic model animal, the zebrafish Danio rerio. doi:10.1016/j.brainres.2004.02.073
- Nakajo H, Chou MY, Kinoshita M, Appelbaum L, Shimazaki H, Tsuboi T, Okamoto H. 2020. Hunger Potentiates the Habenular Winner Pathway for Social Conflict by Orexin-Promoted Biased Alternative Splicing of the AMPA Receptor Gene. *Cell Rep* **31**:107790. doi:10.1016/j.celrep.2020.107790
- Norton WHJ, Folchert A, Bally-Cuif L. 2008. Comparative analysis of serotonin receptor (HTR1A/HTR1B families) and transporter (slc6a4a/b) gene expression in the zebrafish brain. *J Comp Neurol* **511**:521–542. doi:10.1002/cne.21831
- Orger MB, de Polavieja GG. 2017. Zebrafish Behavior: Opportunities and Challenges. *Annu Rev Neurosci* **40**:125–147. doi:10.1146/annurev-neuro-071714-033857

- Pantoja C, Larsch J, Laurell E, Marquart G, Kunst M, Baier H. 2020. Rapid Effects of Selection on Brain-wide Activity and Behavior. *Curr Biol*. doi:10.1016/j.cub.2020.06.086
- Parichy DM. 2015. Advancing biology through a deeper understanding of zebrafish ecology and evolution. *Elife*. doi:10.7554/eLife.05635
- Pistocchi A, Gaudenzi G, Carra S, Bresciani E, Del Giacco L, Cotelli F. 2008. Crucial role of zebrafish *prox1* in hypothalamic catecholaminergic neurons development. *BMC Dev Biol* **8**:27. doi:10.1186/1471-213X-8-27
- Pitrone PG, Schindelin J, Stuyvenberg L, Preibisch S, Weber M, Eliceiri KW, Huisken J, Tomancak P. 2013. OpenSPIM: An open-access light-sheet microscopy platform. *Nat Methods*. doi:10.1038/nmeth.2507
- Porter BA, Mueller T. 2020. The Zebrafish Amygdaloid Complex – Functional Ground Plan, Molecular Delineation, and Everted Topology. *Front Neurosci* **14**:608. doi:10.3389/fnins.2020.00608
- Preibisch S, Saalfeld S, Tomancak P. 2009. Globally optimal stitching of tiled 3D microscopic image acquisitions. *Bioinforma Appl NOTE* **25**:1463–1465. doi:10.1093/bioinformatics/btp184
- Randlett O, Haesemeyer M, Forkin G, Shoenhard H, Schier AF, Engert F, Granato M. 2019. Distributed Plasticity Drives Visual Habituation Learning in Larval Zebrafish. *Curr Biol*. doi:10.1016/j.cub.2019.02.039
- Randlett O, Wee CL, Naumann EA, Nnaemeka O, Schoppik D, Fitzgerald JE, Portugues R, Lacoste AMB, Riegler C, Engert F, Schier AF. 2015. Whole-brain activity mapping onto a zebrafish brain atlas. *Nat Methods* **12**:1039–1046. doi:10.1038/nmeth.3581
- Renier N, Adams EL, Kirst C, Wu Z, Azevedo R, Kohl J, Autry AE, Kadiri L, Umadevi Venkataraju K, Zhou Y, Wang VX, Tang CY, Olsen O, Dulac C, Osten P, Tessier-Lavigne M. 2016. Mapping of Brain Activity by Automated Volume Analysis of Immediate Early Genes. *Cell* **165**:1789–1802. doi:10.1016/j.cell.2016.05.007
- Reveley C, Gruslys A, Ye FQ, Glen D, Samaha J, E. Russ B, Saad Z, K. Seth A, Leopold DA, Saleem KS. 2016. Three-Dimensional Digital Template Atlas of the Macaque Brain. *Cereb Cortex* **27**:4463–4477. doi:10.1093/cercor/bhw248
- Reynaud EG, Peychl J, Huisken J, Tomancak P. 2014. Guide to light-sheet microscopy for adventurous biologists, Nature Publishing Group. doi:10.1038/nmeth.3222
- Richardson DS, Lichtman JW. 2015. Clarifying Tissue Clearing. *Cell*. doi:10.1016/j.cell.2015.06.067
- Rink E, Wullmann MF. 2001. The teleostean (zebrafish) dopaminergic system ascending to the subpallium (striatum) is located in the basal diencephalon (posterior tuberculum). *Brain Res* **889**:316–330. doi:10.1016/S0006-8993(00)03174-7
- Ronneberger O, Liu K, Rath M, Rue D, Mueller T, Skibbe H, Drayer B, Schmidt T, Filippi A, Nitschke R, Brox T, Burkhardt H, Driever W. 2012. ViBE-Z: A framework for 3D virtual colocalization analysis in zebrafish larval brains. *Nat Methods* **9**:735–742. doi:10.1038/nmeth.2076
- Sakai C, Ijaz S, Hoffman EJ. 2018. Zebrafish Models of Neurodevelopmental Disorders: Past, Present, and Future. *Front Mol Neurosci*. doi:10.3389/fnmol.2018.00294

- Schmidt H. 2012. Three functional facets of calbindin D-28k. *Front Mol Neurosci* **5**:25. doi:10.3389/fnmol.2012.00025
- Steadman PE, Ellegood J, Szulc KU, Turnbull DH, Joyner AL, Henkelman RM, Lerch JP. 2014. Genetic effects on cerebellar structure across mouse models of autism using a magnetic resonance imaging atlas. *Autism Res* **7**:124–137. doi:10.1002/aur.1344
- Tabor KM, Marquart GD, Hurt C, Smith TS, Geoca AK, Bhandiwad AA, Subedi A, Sinclair JL, Rose HM, Polys NF, Burgess HA. 2019. Brain-wide cellular resolution imaging of cre transgenic zebrafish lines for functional circuit-mapping. *Elife* **8**. doi:10.7554/eLife.42687
- Ullmann JFP, Cowin G, Kurniawan ND, Collin SP. 2010. A three-dimensional digital atlas of the zebrafish brain. *Neuroimage* **51**:76–82. doi:10.1016/j.neuroimage.2010.01.086
- Vetere G, Kenney JW, Tran LM, Xia F, Steadman PE, Parkinson J, Josselyn SA, Frankland PW. 2017. Chemogenetic Interrogation of a Brain-wide Fear Memory Network in Mice. *Neuron* **94**:363–374.e4. doi:10.1016/j.neuron.2017.03.037
- von Krogh K, Sørensen C, Nilsson GE, Øverli Ø. 2010. Forebrain cell proliferation, behavior, and physiology of zebrafish, *Danio rerio*, kept in enriched or barren environments. *Physiol Behav* **101**:32–39. doi:10.1016/j.physbeh.2010.04.003
- von Trotha JW, Vernier P, Bally-Cuif L. 2014. Emotions and motivated behavior converge on an amygdala-like structure in the zebrafish. *Eur J Neurosci* **40**:3302–3315. doi:10.1111/ejn.12692
- Wang Q, Ding SL, Li Y, Royall J, Feng D, Lesnar P, Graddis N, Naeemi M, Facer B, Ho A, Dolbeare T, Blanchard B, Dee N, Wakeman W, Hirokawa KE, Szafer A, Sunkin SM, Oh SW, Bernard A, Phillips JW, Hawrylycz M, Koch C, Zeng H, Harris JA, Ng L. 2020. The Allen Mouse Brain Common Coordinate Framework: A 3D Reference Atlas. *Cell* **181**:936–953.e20. doi:10.1016/j.cell.2020.04.007
- Wheeler AL, Teixeira CM, Wang AH, Xiong X, Kovacevic N, Lerch JP, McIntosh AR, Parkinson J, Frankland PW. 2013. Identification of a functional connectome for long-term fear memory in mice. *PLoS Comput Biol* **9**:e1002853.
- Wulliman MF, Rupp B, Reichert H. 1996. Neuroanatomy of the zebrafish brain: a topological atlas. Birkhäuser.
- Wullimann MF, Puelles L. 1999. Postembryonic neural proliferation in the zebrafish forebrain and its relationship to prosomeric domains. *Anat Embryol (Berl)* **199**:329–348. doi:10.1007/s004290050232
- Wullimann MF, Rupp B, Reichert H. 1996. Neuroanatomy of the Zebrafish Brain: A Topological Atlas, Neuroanatomy of the Zebrafish Brain. Birkhäuser Verlag, Basel. doi:10.1007/978-3-0348-8979-7
- Xi Y, Noble S, Ekker M. 2011. Modeling neurodegeneration in zebrafish. *Curr Neurol Neurosci Rep* **11**:274–282. doi:10.1007/s11910-011-0182-2
- Yamamoto K, Ruuskanen JO, Wullimann MF, Vernier P. 2010. Two tyrosine hydroxylase genes in vertebrates. New dopaminergic territories revealed in the zebrafish brain. *Mol Cell Neurosci* **43**:394–402. doi:10.1016/j.mcn.2010.01.006
- Yartsev MM. 2017. The emperor’s new wardrobe: Rebalancing diversity of animal models in neuroscience research. *Science (80-)* **358**:466–469. doi:10.1126/science.aan8865

Yushkevich PA, Pashchinskiy A, Oguz I, Mohan S, Schmitt JE, Stein JM, Zukić D, Vicory J, McCormick M, Yushkevich N, Schwartz N, Gao Y, Gerig G. 2019. User-Guided Segmentation of Multi-modality Medical Imaging Datasets with ITK-SNAP. *Neuroinformatics* **17**:83–102. doi:10.1007/s12021-018-9385-x

Supplemental Information

Table S1: Stains

Label	Source	Cat #	Concentration
TO-PRO3 Iodide	Invitrogen	T3605	1:10,000
Primary Antibodies			
Anti-TH	Aves	TYH	1:200
Anti-GFAP	ZIRC	Zrf-1	1:200
Anti-ChAT	Millipore	AB144	1:400
Anti-5-HT	Sigma	S5545	1:100
Anti-Calbindin	SWANT	CB38a	1:200
Anti-Calretinin	SWANT	6B3	1:400
Anti-PCNA	Dako	M0879	1:1000
Anti-HuCD	Invitrogen	A-21271	3.75 µg/mL
Anti-Prox1	Millipore	AB5475	1:400
Anti-Parvalbumin	SWANT	PV27	1:400
Secondary Antibodies			
Donkey anti-mouse Alexa Flour 647	Invitrogen	A31571	1:200
Donkey anti-rabbit Alexa Flour 647	Invitrogen	A31573	1:200
Donkey anti-goat Alexa Flour 647	Invitrogen	A21447	1:200
Goat anti-chicken Alexa Flour 633	Invitrogen	A21103	1:200

Table S2: Brain region abbreviations
















Abbreviation	Full name	Color
A	anterior thalamic nucleus	
AC	anterior cerebellar tract	
ALLN	anterior lateral line nerves	
AON	anterior octaval nucleus	
APN	accessory pretectal nucleus	
ATN	anterior tuberal nucleus	
BSTa	bed nucleus of the stria terminalis, anterior division	
BSTm	bed nucleus of the stria terminalis, medial division	
BSTpd	bed nucleus of the stria terminalis, posterior division	
C	central canal	
Cans	ansulate commissure	
Cantd	anterior commissure, dorsal part	
Cantv	anterior commissure, ventral part	
CC	cerebellar crest	
CCe (granular layer)	cerebellar corpus, granular layer	
CCe (molecular layer)	cerebellar corpus, molecular layer	
Ccer	cerebellar commissure	
Cgus	commissure of the secondary gustatory nuclei	
Chab	habenular commissure	
Chor	horizontal commissure	
CIL	central nucleus of the inferior lobe	
Cinf	commissura infima of Haller	
CM	mammillary body	
CO	optic chiasm	
CON	caudal octavolateralis nucleus	
CP	central posterior thalamic nucleus	
CPN	central pretectal nucleus	
CPop	supraoptic commissure	
Cpost	posterior commissure	
Ctec	tectal commissure	
Ctub	commissure of the posterior tuberculum	
Cven	ventral rhombencephalic commissure	
DAO	dorsal accessory optic nucleus	
Dc	central zone of dorsal telencephalon area	
Dd	dorsal zone of dorsal telencephalon area	
DH	dorsal horn	
DIL	diffuse nucleus of the inferior lobe	
DiV	diencephalic ventricle	

DIV	trochlear decussation	
DI	lateral zone of the dorsal telencephalon	
Dm	medial zone of dorsal telencephalon	
DON	descending octaval nucleus	
DOT	dorsomedial optic tract	
Dp	posterior zone of dorsal telencephalon area	
DP	dorsal posterior thalamic nucleus	
DR	dorsal root	
DTN	dorsal tegmental nucleus	
DV	descending trigeminal root	
E	epiphysis	
ECL	external cellular layer of olfactory bulb	
EG	granular eminence	
EmTI	lateral thalamic eminence	
EmTm	medial thalamic eminence	
EmTr	rostral thalamic eminence	
ENd	entopeduncular nucleus, dorsal part	
ENv	entopeduncular nucleus, ventral part	
EW	Edwinger-Westphal nucleus	
Fld	dorsal part of lateral funiculus	
Flv	ventral part of lateral funiculus	
FR	habenulo-interpeduncular tract	
Fv	ventral funiculus	
GC	central gray	
GL	glomerular layer of olfactory bulb	
Had	dorsal habenular nucleus	
Hav	ventral habenular nucleus	
Hc	caudal zone of periventricular hypothalamus	
Hd	dorsal zone of periventricular hypothalamus	
Hv	ventral zone of periventricular hypothalamus	
I (thalamus)	Intermediate thalamic nucleus	
IAF	inner arcuate fibers	
IC	intercalated nucleus	
ICL	internal cellular layer of olfactory bulb	
IMRF	intermediate reticular formation	
IN	Intermediate nucleus	
IO	inferior olive	
IR	inferior raphe	
IRF	inferior reticular formation	
LC	locus coeruleus	
LCa	caudal lobe of cerebellum	

LFB	lateral forebrain bundle	
LH	lateral hypothalamic nucleus	
LLF	lateral longitudinal fascicle	
LOT	lateral olfactory tract	
LR	lateral recess of diencephalic ventricle	
LRN	lateral reticular nucleus	
MA	Mauthner axon	
MAC	Mauthner cell	
MaON	magnocellular octaval nucleus	
MFB	medial forebrain bundle	
MFN	medial funicular nucleus	
MLF	medial longitudinal fascicle	
MO	medulla oblongata	
MON	medial octavolateralis nucleus	
MOT	medial olfactory tract	
NC	commissural nucleus of Cajal	
NDV	nucleus of the descending trigeminal root	
NI	isthmus nucleus	
NIn	interpeduncular nucleus	
NLL	nucleus of the lateral lemniscus	
nLOT-a	nucleus of the lateral olfactory tract, anterior part	
nLOT-i	nucleus of the lateral olfactory tract, intermediate part	
nLOT-p	nucleus of the lateral olfactory tract, posterior part	
NLV	nucleus lateralis valvulae	
NMLF	nucleus of the medial longitudinal fascicle	
NR	red nucleus	
OENc	octavolateralis efferent neurons, caudal part	
OENr	octavolateralis efferent neurons, rostral part	
OT	Optic tract	
P	posterior thalamic nucleus	
PC	posterior cerebellar tract	
PCN	paracommissural nucleus	
PGa	anterior preglomerular nucleus	
PGc	caudal preglomerular nucleus	
PGl	lateral preglomerular nucleus	
PGm	medial preglomerular nucleus	
PGZ	periventricular gray zone of optic tectum	
Pit	hypophysis	
PL	perilemniscal nucleus	
PLLN	posterior lateral line nerve	
PM	magnocellular preoptic nucleus	

PMg	gigantocellular part of magnocellular preoptic nucleus	
PO	posterior pretectal nucleus	
POF	primary olfactory fiber layer	
PON	posterior octaval nucleus	
PPa	parvocellular preoptic nucleus, anterior part	
PPd	periventricular pretectal nucleus, dorsal part	
PPp	parvocellular preoptic nucleus, posterior part	
PPv	periventricular pretectal nucleus, ventral part	
PR	posterior recess of diencephalic ventricle	
PSm	magnocellular superficial pretectal nucleus	
PSp	parvocellular superficial pretectal nucleus	
PTN	posterior tuberal nucleus	
PVO	paraventricular organ	
R	rostromedial nucleus	
RT	rostral tegmental nucleus	
RV	rhombencephalic ventricle	
SC	suprachiasmatic nucleus	
SCO	subcommissural organ	
SD	dorsal sac	
SG	subglomerular nucleus	
SGN	secondary gustatory nucleus	
SGT	secondary gustatory tract	
SO	secondary octaval population	
SR	superior raphe	
SRF	superior reticular formation	
SRN	superior reticular nucleus	
SY	psiloniform sulcus	
T	tangential nucleus	
TBS	bulbo-spinal tract	
TeIV	telencephalic ventricles	
TeO	optic tectum	
TeV	tectal ventricle	
TGN	tertiary gustatory nucleus	
TL	longitudinal torus	
TLa	lateral torus	
TMCa	anterior mesencephalocerebellar tract	
TMCP	posterior mesencephalocerebellar tract	
TPM	pretecto-mammillary tract	
TPp	periventricular nucleus of posterior tuberculum	
TSc	central nucleus of semicircular torus	
TSvl	ventrolateral nucleus of semicircular torus	

TTB	tractus tectobulbaris	
TTBc	crossed tecto-bulbar tract	
TTBr	uncrossed tecto-bulbar tract	
TVS	vestibulo-spinal tract	
Val (granular layer)	lateral division of valvula cerebelli, granular layer	
Val (molecular layer)	lateral division of valvula cerebelli, molecular layer	
Vam (granular layer)	medial division of valvula cerebelli, granular layer	
Vam (molecular layer)	medial division of valvula cerebelli, molecular layer	
VAO	ventral accessory optic nucleus	
Vas	vascular lacuna of area postrema	
Vc	central nucleus of ventral telencephalon area	
Vd-dd	dorsal zone of ventral telencephalon	
Vd-vd	ventral zone of ventral telencephalon	
Vdd	dorsal most zone of ventral telencephalon	
VH	ventral horn	
VI	lateral nucleus of ventral telencephalon	
VL	ventrolateral thalamic nucleus	
VM	ventromedial thalamic nucleus	
VOT	ventrolateral optic tract	
Vp	postcommissural nucleus of ventral telencephalon	
Vs	supracommissural nucleus of ventral telencephalon	
Vv	ventral nucleus of ventral telencephalon	
ZL	zona limitans	
I	olfactory nerve	
II	optic nerve	
III	oculomotor nerve	
III _m	oculomotor nucleus	
IV	trochlear nerve	
IV _m	trochlear nucleus	
V	trigeminal nerve	
V _{md}	trigeminal motor nucleus, dorsal part	
V _{md}	dorsal motor root of the trigeminal nerve	
V _{mn}	mesencephalic nucleus of the trigeminal nerve	
V _{mv}	trigeminal motor nucleus, ventral part	
V _{mv}	ventral motor root of the trigeminal nerve	
V _{mvr}	ventral trigeminal motor root	
V _{sm}	primary sensory trigeminal nucleus	
V _{sr}	sensory root of the trigeminal nerve	
VI	abducens nerve	
VI _c	caudal root of the abducens nerve	
VI _{mc}	abducens nucleus, caudal part	

Vlmc	caudal abducens nerve motor nucleus	
Vlmr	rostral abducens nerve motor nucleus	
Vlr	rostral root of the abducens nerve	
VII	facial nerve	
VII Lo	facial lobe	
VII m	facial motor nucleus	
VII mr	facial motor root	
VII s	sensory root of the facial nerve	
VIII	octaval nerve	
IX	glossopharyngeal nerve	
IX Lo	glossopharyngeal lobe	
IX m	glossopharyngeal nerve motor nucleus	
X	vagal nerve	
X Lo	vagal lobe	
X m	vagal motor nucleus	

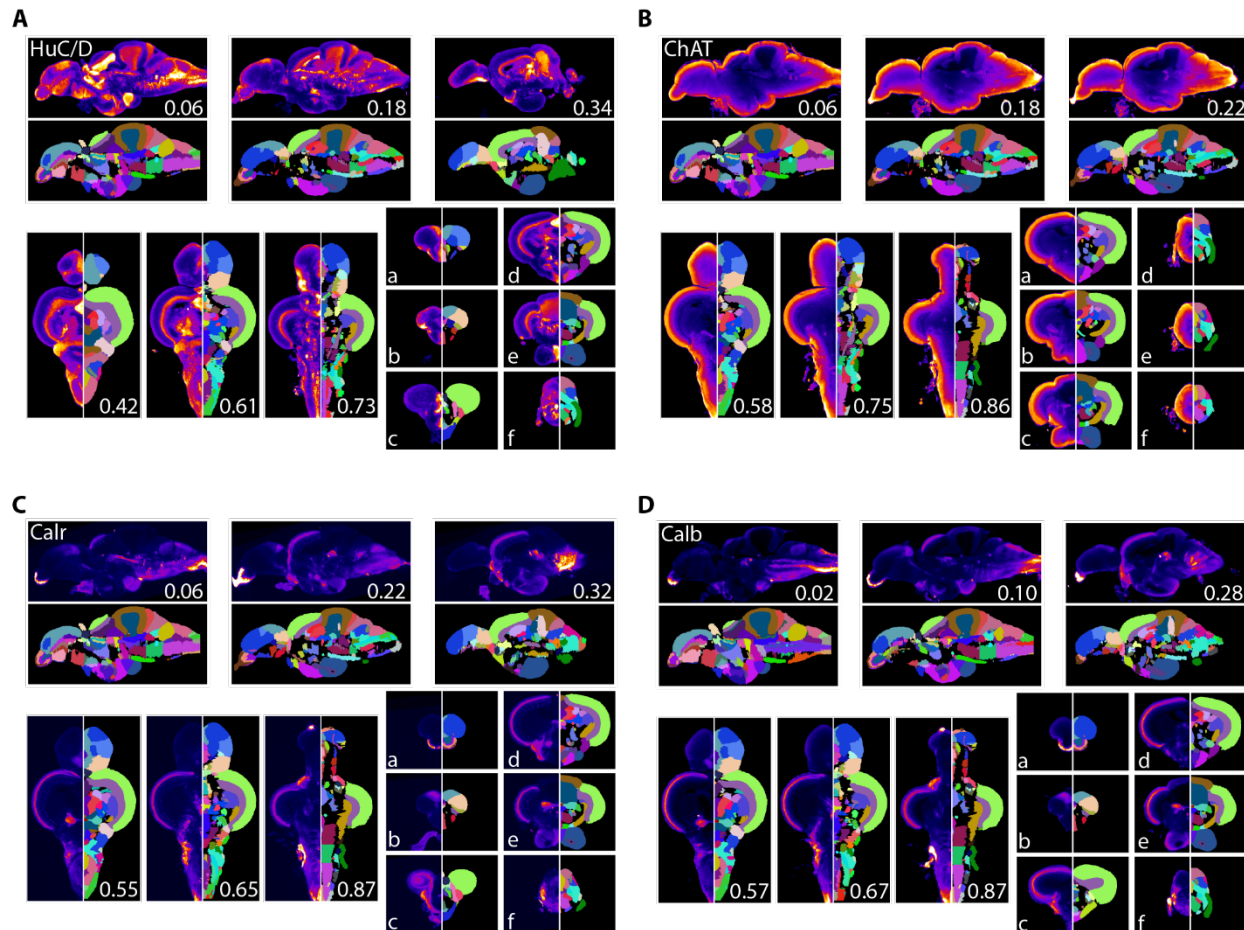


Figure S1. Averaged and registered antibody stains with corresponding segmentation for **A)** HuC/D, **B)** ChAT, **C)** Calretinin (Calr), and **D)** Calbindin (Calb) where hotter colors indicate greater staining. For sagittal (top) and horizontal (left, bottom) numbers represent distance (in mm) from midline or top of the brain, respectively. Slices for each plane were chosen based on the presence of staining (see results for description).